A Climatology of the Aleutian High

V. LYNN HARVEY AND MATTHEW H. HITCHMAN

Department of Atmospheric and Oceanic Sciences, University of Wisconsin—Madison, Madison, Wisconsin

(Manuscript received 16 June 1995, in final form 31 January 1996)

ABSTRACT

Three global datasets are used to investigate climatological properties of the high pressure system commonly found in the boreal winter stratosphere over the Aleutian Islands. Based on a detailed examination of 10 years (1985–1994) of data from the European Centre for Medium-Range Weather Forecasts in the layer 250–10 hPa, the following definition of the "Aleutian High" is proposed: 1) 10-hPa heights exceeding 30.8 km in the sector 40°–80°N, 120°E–100°W, 2) during 1 October–31 March, 3) with areal extent greater than 50° long × 10° lat., 4) with relative vorticity of less than -2.5×10^{-5} s^{-1}, and 5) lasting at least 5 days. More than 60% of days during December, January, and February satisfied these criteria. The 711 total days were averaged together, yielding an Aleutian High Composite (AHC). These ECMWF dates are used to create an AHC with data from the National Centers for Environmental Prediction (formerly the National Meteorological Center.) The definition is applied (with slight modification) to the data from the Limb Infrared Monitor of the Stratosphere experiment, allowing extension into the mesosphere. The AHC structures of geopotential height, temperature, winds, and potential vorticity are examined in detail, and differences among the composites are discussed.

The Aleutian High and polar vortex constitute a ridge/trough pair that tilts westward with altitude from the surface into the mesosphere. The geopotential height difference between the Aleutian high and the polar vortex maximizes at ~3 km near the stratopause. Warm and cold temperature perturbations underly these features to the west, giving rise to a poleward heat flux. Axes of high heights and warm air trend continuously equatorward and downward into the subtropical western Pacific.

During much of the boreal winter, stratospheric and mesospheric flows are highly zonally asymmetric. At 10 hPa the AHC structure shows zonal eastward flows of less than 10 m s^{-1} near 180°, but greater than 40 m s^{-1} near 80°E, with ~20 m s^{-1} northward flow near 130°E and southward flow near 100°W. Parcel descent rates exceeding 2 km day^{-1} are diagnosed ~60° upstream of the warm anomaly. The Aleutian High thus helps determine preferred longitude bands of winter subsidence and of material exchange between the subtropics and extratropics.

1. Introduction

Useful conceptual advances have been made by regarding the middle atmosphere as primarily zonally symmetric and examining departures from a zonal mean state. A complementary paradigm emphasizes the notable zonal asymmetries that are prevalent in observations, even in seasonal averages. Quasi-stationary continental-scale circulations play a major role in the annual cycle of the tropical and subtropical stratosphere and affect the southern winter flow (Postel 1994). These chronic zonal asymmetries in the south polar vortex during austral winter are visible in distributions of total ozone as measured by the Total Ozone Mapping Spectrometer (TOMS) instrument (Bowman and Krueger 1985). Perhaps the best-studied zonally asymmetric feature is the anticyclone that dominates the stratosphere over the North Pacific during boreal winter. Near 10 hPa, maximum geopotential heights are usually found over the Aleutian Islands near 55°N, 175°W. This phenomenon has come to be known as the Aleutian high (hereafter AH). A variety of observational studies have explored its structure and behavior during various winters (e.g., Stroud et al. 1959; Wilson and Godson 1963; Labitzke 1972, 1977, 1980, 1981, 1982; Hirota et al. 1973; van Loon et al. 1975; Wallace and Gutzler 1980). The accumulation of many years of global meteorological fields for the middle atmosphere presents an opportunity to explore the statistical properties of the AH. This paper offers criteria for determining when the AH is present and documents its composite structure, as a contribution toward a geographical description of the stratosphere, and as a basis for model comparison and theoretical interpretation.

A complete dynamical explanation for this warm stratospheric ridge remains elusive. Some early suggestions include an infrared transfer connection with the warm North Pacific sea surface (Boville 1963), subsidence in the lower stratosphere associated with the indirect circulation of the subtropical jet (Kitaoka

Corresponding author address: V. Lynn Harvey, Department of Atmospheric and Oceanic Sciences, University of Wisconsin—Madison, 1225 W. Dayton Street, Madison, WI 53706.
E-mail: lynn@meteor.wisc.edu

1963) or with cyclogenesis (Boville 1960; Finger and Teweles 1963), and baroclinic instability (Teweles 1958; Fleagle 1958; Boville 1960, 1963). The upward extension of planetary waves with tropospheric sources (Charney and Drazin 1961) has been invoked to explain its apparent connection to the ridge over the west coast of North America, westward tilt with altitude, and variability. Indeed, variability in the AH seems to be intimately connected to variability of the strength and position of the polar vortex (Dickinson 1968; Farman et al. 1994), sudden stratospheric warming events (SSWs), and tropospheric blocking events (Julian 1963; Julian and Labitzke 1965; Wada 1968; Quiroz 1986; Juckes and O'Neill 1988). A synoptic description of a SSW includes the migration of a warm anticyclone sufficiently close to the pole as to cause zonal mean winds to become easterly. It is thus sometimes challenging to distinguish the AH and SSW phenomena.

A number of numerical and theoretical investigations have attempted to assess the relative importance of various radiative and dynamical processes affecting stratospheric planetary waves (Kasahara et al. 1973; Hoskins and Karoly 1981; Plumb 1985; Butchart and Remsberg 1986; O'Neill and Pope 1993; Pierce et al. 1993). O'Neill and Pope showed convincingly that the AH is fundamentally nonlinear in that large wave amplitude forcing in the troposphere will generally yield the observed pattern. They also elucidated the viewpoint that it is often more insightful to regard the situation as two interacting vorticies, instead of as a wave-mean flow interaction problem. Global forcing patterns have also been linked to variability in the AH region, including the quasi-biennial oscillation (QBO) (Holton and Tan 1980, 1982; Labitzke 1982; Wallace and Chang 1982; van Loon and Labitzke 1987; Dunkerton et al. 1988), the El Niño–Southern Oscillation (ENSO) (e.g., Hamilton 1993a,b), solar cycle (e.g., Labitzke 1981), and other teleconnection patterns (van Loon and Shea 1992; Baldwin et al. 1994; Baldwin and O'Sullivan 1995; Perlwitz and Graf 1995).

Stratospheric anticyclones have been found to be an essential aspect of planetary wave breaking, irreversible mixing, and the associated advection of tropical isentropic potential vorticity (PV) to higher latitudes (McIntyre and Palmer 1983, 1984; Dunkerton and Delisi 1986; Fairlie et al. 1990; Randel et al. 1993; Waugh 1993; Manney et al. 1994b; Plumb et al. 1994; Waugh et al. 1994; O'Neill et al. 1994). One useful conceptual model is the vortex-vortex oscillator, where the polar low is maintained radiatively, but when disturbed, extracts low PV air from the Tropics, amplifying the AH through "accretion," which displaces the low toward the Tropics again. Other investigators have emphasized that the upward transmissivity of wave activity depends on the temperature and wind structure near the tropopause (Karoly and Hoskins 1982; Lin 1982; Shiotani 1986; Nigam and Lindzen 1989; Chen and Robinson 1992; Da Silva and Lindzen 1993). McIntyre (1982) gives a comprehensive discussion of many of the processes related to SSWs and stratospheric disturbances.

The complexity of interrelationships between stratospheric anticyclones over the North Pacific and these other phenomena make it very challenging to diagnose their underlying cause. Here we adopt the philosophy that it is worthwhile to define the AH quantitatively in order to isolate and study it as a distinct entity. This approach surely oversimplifies the situation, but proves to be useful in defining the typical structure of the AH. This work is similar in spirit to that of (Hartmann and Ghan 1980) in their compositing of tropospheric blocking events.

In defining and documenting the AH, we first employed a decade (1985–1994) of data from the European Centre for Medium-Range Weather Forecasts (ECMWF). To explore the AH structure above 10 hPa, we then analyzed data from the National Meteorological Center (NMC, now referred to as the National Centers for Environmental Prediction) and data from the Limb Infrared Monitor of the Stratosphere (LIMS) experiment. These datasets and analysis methods are described in section 2. Longitude–time diagrams of 10-hPa geopotential height for two different winters are then shown to illustrate the large variability that is typically encountered and the challenges in attempting to define the AH (section 3). Our proposed definition of the AH is given in section 4. The resulting ECMWF composite at 10 hPa is discussed in section 5. Longitude–altitude and latitude–altitude perspectives of AH composites for all three datasets are analyzed and compared in sections 6 and 7. The deep vertical extent into the mesosphere, connection with the troposphere, and broad latitudinal extent are emphasized. We are currently working on a more thorough study of dynamical mechanisms as a complement to this climatological study, although here we include initial estimates of temperature advection and comment on implications for parcel heating rates. A summary and conclusions are given in section 8.

2. Data and analysis

Due to the variety of types of observations included and care in assimilation procedures, ECMWF data were chosen as the primary product for climatological studies of the AH. Trenberth (1992) provides a discussion of the observation types, assimilation methods, and data quality for the ECMWF data. Significant quality enhancement occurred beginning in 1985, so the period 1985–1994 was chosen. Analyzed ECMWF fields of temperature, geopotential height, and the three wind components were acquired from the National Center for Atmospheric Research, for the eight pressure levels 250, 200, 150, 100, 70, 50, 30, and 10 hPa, at a meridional resolution of 2.5°, and 18 zonal wavenumbers.

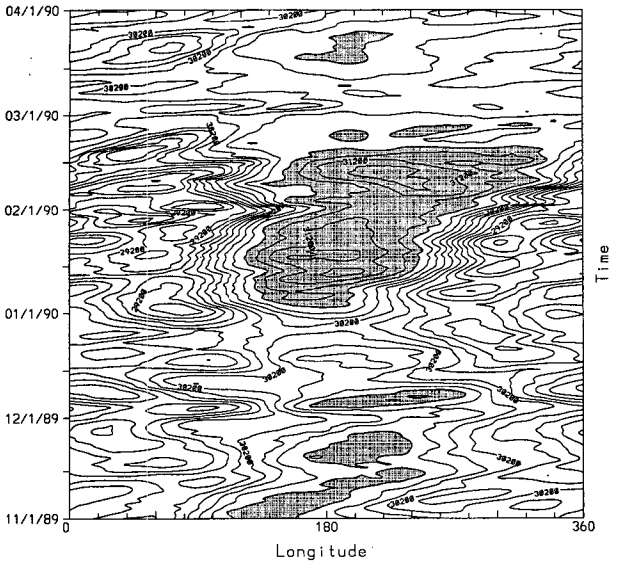

FIG. 1. Longitude–time section of geopotential height at 10 hPa and 55°N for the period 1 November 1989–1 April 1990. Contour interval is 200 m. Geopotential heights exceeding that of criteria (1), which is 30.8 km, are shaded.

To determine the structure of the AH above 10 hPa, and to have a self-consistent extension to the surface within one dataset, we also employed NMC data for the same period, 1985–1994. Details of the NMC products are given by Trenberth and Olson (1988). NMC fields of temperature and geopotential height were obtained from the Langley Research Center at the 16 pressure levels 1000, 500, 400, 300, 250, 200, 150, 100, 70, 50, 30, 10, 5, 2, 1, and 0.4 hPa (temperature only to 1 hPa), at a meridional resolution of 4°, and 18 zonal wavenumbers. NMC horizontal wind components were calculated from the available geopotential height field using geostrophic balance and centered finite differencing. To compare results obtained from the ECMWF and NMC datasets, the ECMWF composite data was linearly interpolated from a 2.5° to a 4° latitudinal resolution.

Since the LIMS instrument sampled well into the mesosphere at high vertical resolution (~3 km), we also examined the structure of the AH in this dataset. Gille and Russell (1984) describe general qualities of the LIMS data. Version 4 mapped temperature and geopotential height values were used, as described by Hitchman and Leovy (1986), at the 18 levels 100, 70, 50, 30, 16, 10, 7, 5, 3, 2, 1.5, 1, 0.7, 0.5, 0.4, 0.2, 0.1, and 0.05 hPa, with 4° meridional resolution from 64°S to 84°N, and zonal wavenumber 6 truncation. This dataset spans the period 25 October 1978–28 May 1979, providing a view of the AH during a different, rather disturbed, winter.

Zonal harmonic values were projected onto a grid with a zonal resolution of 9.7°. This is comparable to the effective resolution of the harmonic coefficients for the ECMWF and NMC data, but the effective grid spacing of the LIMS data is actually about 25°.

The contributions of three-dimensional temperature advection, $-u\delta T/\delta x - v\delta T/\delta y - w\delta T/\delta z$ (using centered differencing), and of adiabatic motion, $-g/C_p w$, to the local temperature tendency will be shown. Since the AHC is a time-averaged structure the sum of these terms gives an estimate of the rate of temperature change experienced by air parcels in a Lagrangian sense. This, in turn, provides an estimate of the radiative heating or cooling required to maintain the AHC structure.

Ertel's potential vorticity, PV, was calculated in the form $(\zeta + f)1/\rho(\partial\theta/\partial z)$ on pressure surfaces, then linearly interpolated to potential temperature surfaces. Differences in the slopes of pressure and potential temperature surfaces are small enough to introduce only small errors. As described by Lait (1994), due to the rapid upward increase of PV, in horizontal-vertical sections it is sometimes difficult to discern horizontal variations. In presenting fields of PV, we adopted his recommendation of modifying PV by a factor that minimizes this effect: $\Pi = P(\theta/\theta_0)^{-9/2}$.

3. Aleutian High variability

From the composite structures about to be shown it would be easy to get the impression that the AH is characteristically steady. That this is not the case can be seen clearly in Figs. 1 and 2, which contrast the behavior of ECMWF geopotential height at 10 hPa, 55°N during the periods 1 November 1989–1 April 1990 and 1 November 1985–1 April 1986, respectively. Note the shaded regions of high heights near

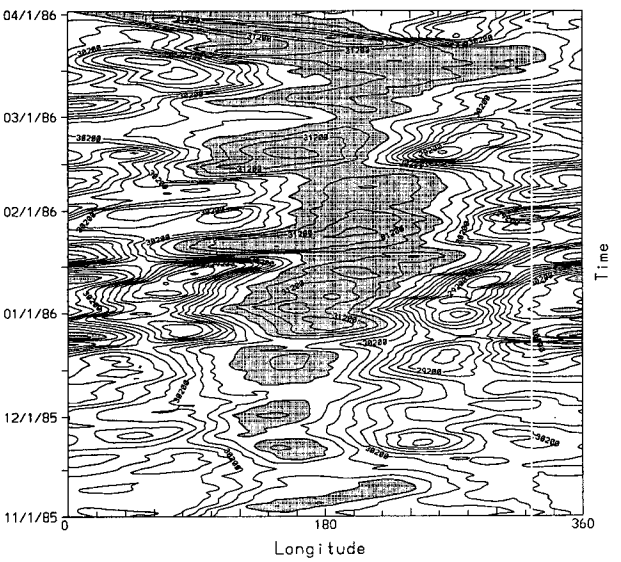

FIG. 2. As Fig. 1 except for winter of 1985/86.

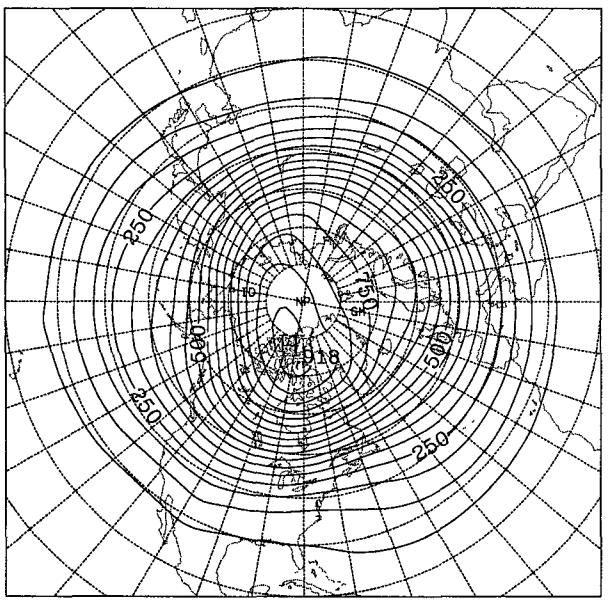

FIG. 3. Polar stereographic map (Northern Hemisphere poleward of 20°N) at 10 hPa of the standard deviation of geopotential height for ECMWF AHC days that occurred in December–January–February. Contour interval is 50 m.

180°E exceeding 30.8 km (an AH is surely present at these times). Considerable week-to-week variability is seen in both winters, but is much more pronounced in the winter of 1985–1986. In 1989–1990 the phenomenon is quite robust and stationary from late December through mid-February, while during 1985–1986 it has a much more sporadic character, recurring throughout the whole period shown, and exhibiting a great deal of zonal propagation. This confirms the findings of (Hirota et al. 1973), who showed that quasi-periodic oscillations of winds over Japan in the upper stratosphere are largely due to spatial variation of the anticyclone center. In late March, the anticyclone propagates rapidly westward (and over the pole, not shown), with the permanent elimination of the polar vortex for the winter. Note also the formation of a second high over the North Atlantic during January, which then propagates eastward. In a sequence of polar stereographic maps (not shown) the two highs merge at an intermediate location near 100°E, then migrate to 180°. This type of "accretion" or "merging" behavior is fairly common. Rosier et al. (1994) and O'Neill et al. (1994) give interesting descriptions of this type of variability during the 1991/92 winter.

The 1989/90 winter, having no major midwinter warming over the pole in the lower stratosphere, could be characterized as cold and undisturbed (Labitzke 1981). It is relatively easy to decide which of these days should be included in an AHC. Incidentally, the characterization cold and undisturbed is only valid for the lower stratosphere and would not necessarily aid in creating a composite at altitudes higher than 10 hPa. For more active winters, such as the 1985/86 winter, the transience and spatial deformation of temperature and geopotential height fields makes this much more difficult. Criteria defining the AH were obtained through careful examination of daily sequences of events in the ECMWF dataset. The criteria reflect a rather conservative approach, where it was decided to exclude dynamically distinct times, such as when the AH was propagating rapidly, during mature stratospheric warmings, or when a robust North Atlantic high was also present.

4. Definition of the Aleutian High

Due to the relative lack of data above 10 hPa, the AH has been associated historically with the 10-hPa surface. It is likely that radiosonde observations will remain a primary source of data, so we chose to define the AH at this level. We suggest the following criteria as a definition for the ECMWF AH, which we used to define the days for creating the AH composites: 1) 10-hPa heights exceeding 30.8 km in the sector 40°–80°N, 120°E–100°W, 2) during 1 October–1 April, 3) with areal extent greater than 50° long. × 10° lat., 4) relative vorticity less than -2.5×10^{-5} s^{-1}, and 5) lasting at least 5 days. All five criteria must have been met for a day to be included in the composite (AH day). The resulting AH days were qualitatively reviewed and a few were rejected, as described below. During January 1985–March 1994 711 out of 1730 October–April days (41%) satisfied this definition.

On each day, the location of highest geopotential height was determined. If that location was outside of the sector in criterion 1, such as when a strong North Atlantic high is present, the day was not included. This method eliminated numerous instances of a strong AH; however, it left the AHC structure more well defined. The sector in criterion 1 was chosen as follows: The northern edge was chosen to try to exclude sudden warmings, while the southern limit excludes subtropical phenomena. There is a degree of overlap between the AH and some SSWs. In "Canadian" warmings the polar vortex is left intact, though displaced far from the pole. Sometimes the maximum height is found equatorward of 80°N and these days were included in the composite. Indeed, this type of warming can be viewed as a quasi-stationary amplification of the AH. When the location of highest heights is found to the east or west of the given sector, it is usually highly transient. Criterion 2 is motivated by the fact that the AH is a winter phenomenon, being distinguished from the summer polar anticyclone (which also has quite high geopotential heights) by its coexistence with the polar low. An AH of substantial area was ensured by criterion 3. Sometimes high heights were observed over a broad area with only a weak anticyclonic circulation, hence criterion 4. This sort of criterion, invoking a relative vor-

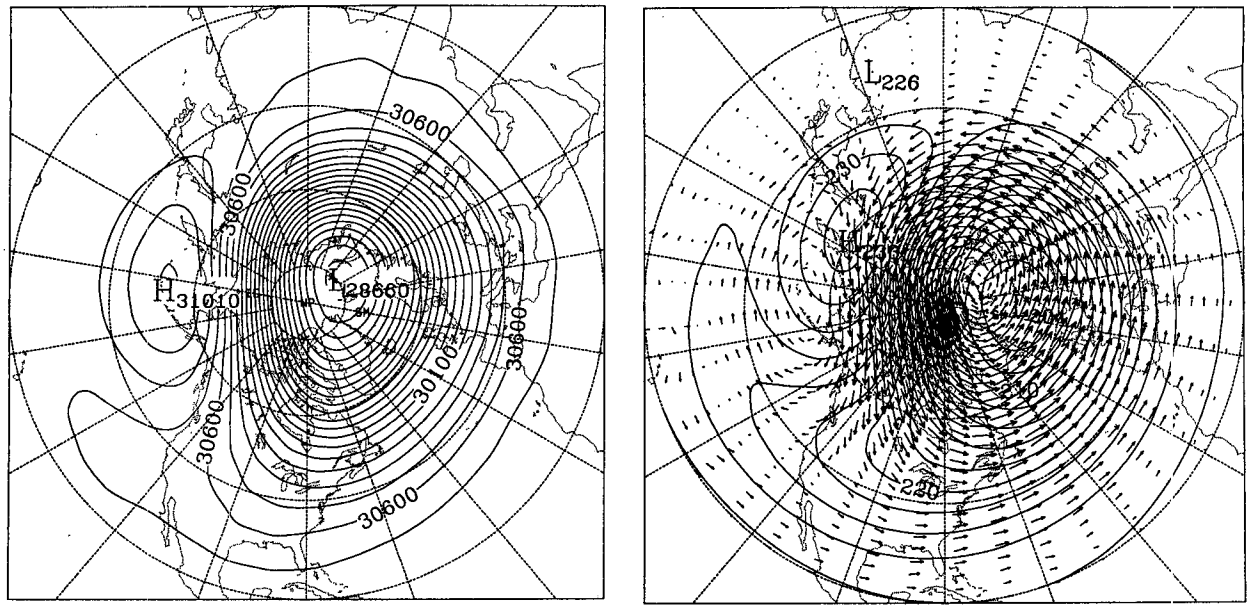

FIG. 4. Polar stereographic map at 10 hPa of the ECMWF AHC (a) geopotential height (contour interval 100 m), and (b) temperature (contour interval 2 K) and horizontal winds. The longest wind vector corresponds to 60 m s^{-1}.

ticity threshhold, has been used to define other phenomena (e.g., Reed et al. 1986). Due to the AH being typically elongated east–west, and due to stronger height gradients to the north than to the south, the relative vorticity was averaged in a 20° long. × 17.5° lat. area centered one-half grid point south of the location of the AH maximum, and compared to the threshold value in criterion 4. Following the work of Hartmann and Ghan (1980), who sought to distinguish transient ridges from blocking highs in the troposphere, we adopt a persistence condition of 5 days. This is perhaps the most stringent, but ensures that the composite excludes highly transient features.

It is important to note the following three situations that were considered in a subjective determination of which days to include in the AHC, factors which other investigators would need to consider in studying the AH. First, there were what we called "rapid retrogression" or "accretion" events, where the AH maximum propagated westward more than 80° in 3 days and subsequently amplified at a different longitude (occasionally upon merging with an eastward propagating North Atlantic high). This occurred eight times during these 10 winters, resulting in 17 total days being omitted. We are examining these events separately to gain insight into the process of advecting low PV air from the Tropics around the polar low. Second, our restriction on sudden warmings or North Atlantic heights exceeding Pacific heights occurred during 13 synoptic events, resulting in the elimination of 87 days from our composite. Third, there were isolated days that barely failed the AH criteria, but were surrounded in time by AH days. These 17 days were added to the AHC. These qualitative adjustments to the 5 criteria yielded the 711 days for analysis in the ECMWF data. These same days were then analyzed in the NMC data to make the NMC AHC. The criteria were applied without qualitative adjustment to the LIMS winter 1978/79 yielding a much smaller sample (53 days). This is commented upon below. The resulting AHC composites comprise a range of synoptic situations, but we feel that this method minimizes differences among days that are included, with the resulting latitudinal and vertical structure being fairly similar among AH days.

Potential vorticity is enjoying a renaissance as a diagnostic tool. It may therefore be desirable to establish PV-based AH criteria. Geopotential height was used here for the fundamental definition since it is less subject to differences between calculation methods. The AHC PV chart to be shown suggests that an alternative definition to criteria 1 and 4 is $P < 1.5 \times 10^{-4}$ K m^2 kg^{-1} s^{-1} (hereafter referred to as 1.5 "PV units") at the 750 K surface.

The distribution of AH days by month for the 1985–1994 record is as follows, with the numbers in parentheses being the number of days in each month and the percent of occurrence out of the total days for that month: October (2, 1%), November (63, 23%), December (171, 61%), January (194, 63%), February (144, 63%), March (136, 44%). The peak occurrence is in January. Although the AH occurrence frequency is larger for December than February, the AH exists more sporadically in December and is more stable in February. The AH days are more common in March

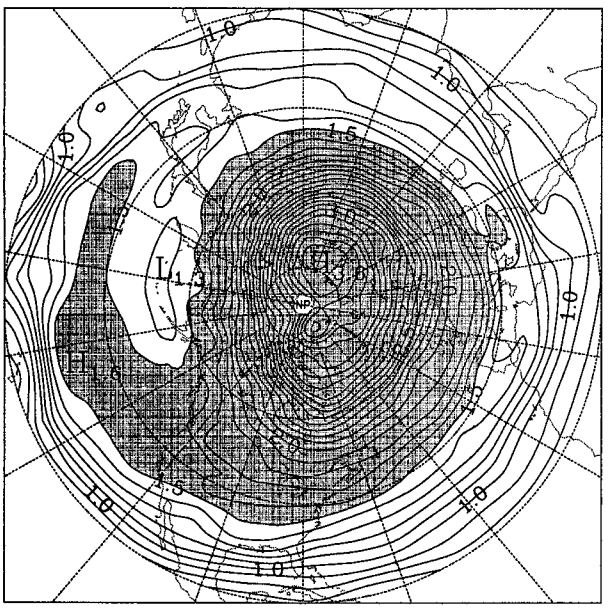

FIG. 5. Polar stereographic map of the ECMWF AHC potential vorticity on the 750 K isentropic surface. High values of PV are shaded. Contour interval is 1×10^{-5} K m^2 K g^{-1} s^{-1}.

than in November, reflecting its relatively greater stability in late winter compared to its formative period. The month of October had only two occurrences in a decade and could have been omitted from the climatology. This is to some degree a result of the phenomena of late winter and final warmings, of which the AH is almost always present. Therefore, the AH is, to an extent, representative of stratospheric winter variability that is caused by warmings.

Since the occurrence of the AH is concentrated largely in December, January, and February (DJF), the question may be raised of whether the DJF mean would capture its essence. We chose to create the AHC by including any winter day with a similar structure. In contrast, many DJF days do not exhibit an AH. A comparison of the AHC with all DJF days reveals that the maximum height and temperature differences are 400 m and 7 K greater in the AHC (which also includes days from other months). For assessing the variability of AH days included in the composite to be discussed in the next section, here we include a plot (Fig. 3) of the standard deviation of geopotential height at 10 hPa for AH days during the DJF period alone. A maximum of 900 m is found over northern Canada, with high values trending between the AH and polar vortex. This is consistent with modest variation in the location of the high/low pair on AH days. This is much smaller than the 2.4-km height difference between the composite AH and polar low at 10 hPa (Fig. 4a). It is interesting to note that this σ pattern is similar to the patterns of the first canonical modes relating 50-hPa heights to 500-hPa heights and to 850-hPa temperatures found by Perlwitz and Graf (1995, cf. their Figs. 4 and 9). In work to be reported elsewhere, the AHC minus DJF mean geopotential height distribution shows an enhanced "Pacific North America" pattern (Wallace and Gutzler 1981) and amplified North Atlantic High, consistent with the idea of forcing the AH via tropospheric longwave amplification.

5. The ECMWF Aleutian High composite at 10 hPa

The ECMWF AHC structure in 10-hPa heights is shown in Fig. 4a. The polar vortex is found characteristically displaced off of the pole near 80°N, 50°E, while the Aleutian High is centered near 55°N, 180°. The difference in altitude for the 10-hPa surface at these locations is ~2.4 km.

The corresponding AHC structure in temperature and horizontal winds is shown in Fig. 4b. A warm center of ~233 K is found ~30° to the west of the AH, while a cold center of ~204 K is found ~40° to the west of the polar low, yielding a temperature difference of 30 K. As will be shown below, this is comparable to vertical temperature differences in many parts of the winter stratosphere. This displacement between temperature and geopotential height centers, or baroclinic signature, is consistent with previous findings (cf. Hirota et al. 1973; Fairlie et al. 1990; O'Neill et al. 1994).

Horizontal winds exhibit a very intense cross-polar flow between the polar low and AH, reaching 60 m s^{-1} in the composite (Fig. 4b). Note the chronic easterly flow near 45°N over the Pacific past Japan, and substantial westerly flow in the midlatitudes of the rest of the hemisphere. Air passing near the pole characteristically moves equatorward over North America, while substantial poleward flow typically occurs over Siberia.

In terms of parcel displacement within this planetary wave pattern, cold air at the apex of its trajectory in the eastern hemisphere, subsides while moving poleward, with compressional heating causing a warm anomaly that underlies the AH hydrostatically. From the nadir in its trajectory, warm air ascends and moves equatorward, with ascent cooling causing a cold anomaly that underlies the polar low hydrostatically. Thus, the poleward heat flux depends very much on the pattern of subsidence and ascent. In undergoing a circuit, parcels are brought in and out of the sunlight, range across several kilometers of altitude, and across tens of degrees in temperature, strongly affecting photochemical reaction rates and composition.

The AHC distribution of PV on the 750 K surface is shown in Fig. 5. High values of PV, which are representative of polar vortex air, are shaded. In the polar vortex values exceed 3 PV units, while they are less than 1.5 in the AH region. A locus of high PV values trends in a spiral out of the polar vortex equatorward across North America and across the Pacific near 35°N, in a classic wave breaking pattern associated with the

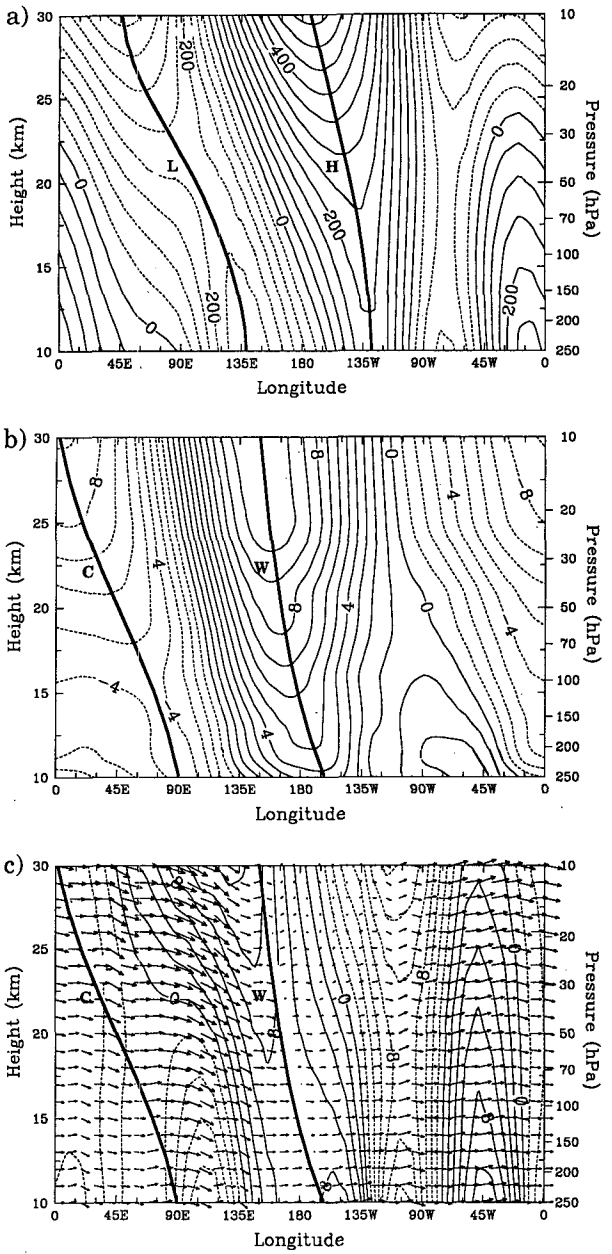

FIG. 6. Longitude–altitude section at 55°N of ECMWF composite (a) eddy (deviation from the zonal mean) geopotential height (contour interval 50 m), (b) eddy temperature (contour interval 1 K), and (c) three-dimensional wind. Zonal and vertical components are shown as vectors (longest vector represents 60 m s^{-1}) where vertical velocities are multiplied by a factor of 1000 for visibility. The meridional component is contoured every 2 m s^{-1}, where poleward flow is shaded. In Figs. 6a and 6b positive eddy values, which associated with the Aleutian high structure, are contoured using solid lines. Axes of high and low heights and of warm and cold temperatures are drawn on Fig. 6a, and Figs. 6b and 6c, respectively.

Aleutian high. A locus of low PV values spirals poleward from the Carribean, across the Mediterranean and central Asia, and out over the Aleutian Islands, suggestive of a pathway of tropical air mass movement, which may help to maintain the low PV nature of the AH.

This "occidental/oriental asymmetry" in meridional mass exchange and the preferred paths for air motion can account for Hofmann and Rosen's (1984) observations of CCN (cloud condensation nuclei) surge events over Laramie, Wyoming. These may represent cores of evaporated volcanic aerosol that were detrained out of the "upper regime" of the tropical volcanic aerosol reservoir (Trepte and Hitchman 1992; Hitchman et al. 1994). In addition to preferred lofting on the summer side of the equator due to ozone heating, the AH structure helps to determine the shape of this upper aerosol regime in the middle stratosphere, which is characterized by lower values on the winter side of the equator.

6. Longitude–altitude structure

The vertically continuous nature of the AH-polar low pair is best illustrated by longitude–altitude sections through the ECMWF AHC at 56°N. Eddy geopotential heights and temperatures are shown in Figs. 6a and 6b. Winds are depicted in Fig. 6c, with arrows indicating the zonal and vertical components, and meridional winds contoured. Primary axes of warm and cold regions are sketched on Fig. 6b, from which it can be seen that cold air underlies the trough and warm air underlies the ridge, with the whole system tilting westward with altitude. Temperature extrema lie 30°–40° to the west of geopotential height maxima. Note how the upper-tropospheric North Atlantic anticyclone wanes with altitude, while the high located near 135°W amplifies upward to 10 hPa. Kaas and Branstator (1993) found that blocking occurs in the upper troposphere over the Canadian rockies for more than 20% of January days. The upper tropospheric trough over the northwestern Pacific also amplifies as it tilts westward with altitude, and there is a suggestion that above 10 hPa it merges with the barotropic trough located over the east coast of North America. The range in eddy temperatures associated with the AH–polar low pair increases from 8 K at 250 hPa to 25 K at 10 hPa.

Axes of warm and cold temperatures are also sketched on Fig. 6c. Southwesterly flow approaching the warm axis subsides at a surprisingly large rate, exceeding 30 mm s^{-1} [compare to results in Manney et al. (1994a)]. Northwesterly flow approaching the cold axis ascends at a more moderate rate at this latitude. Although uncertainties in vertical motion are larger than for the other fields, they have been estimated in a dynamically self-consistent manner and the spatial coherence, location, and magnitude are consistent with the observed temperature structure. The fact should be kept in mind, however, that vertical velocities obtained in a forecast/analysis system like that employed at ECMWF pose serious limitations in dynamical interpretation.

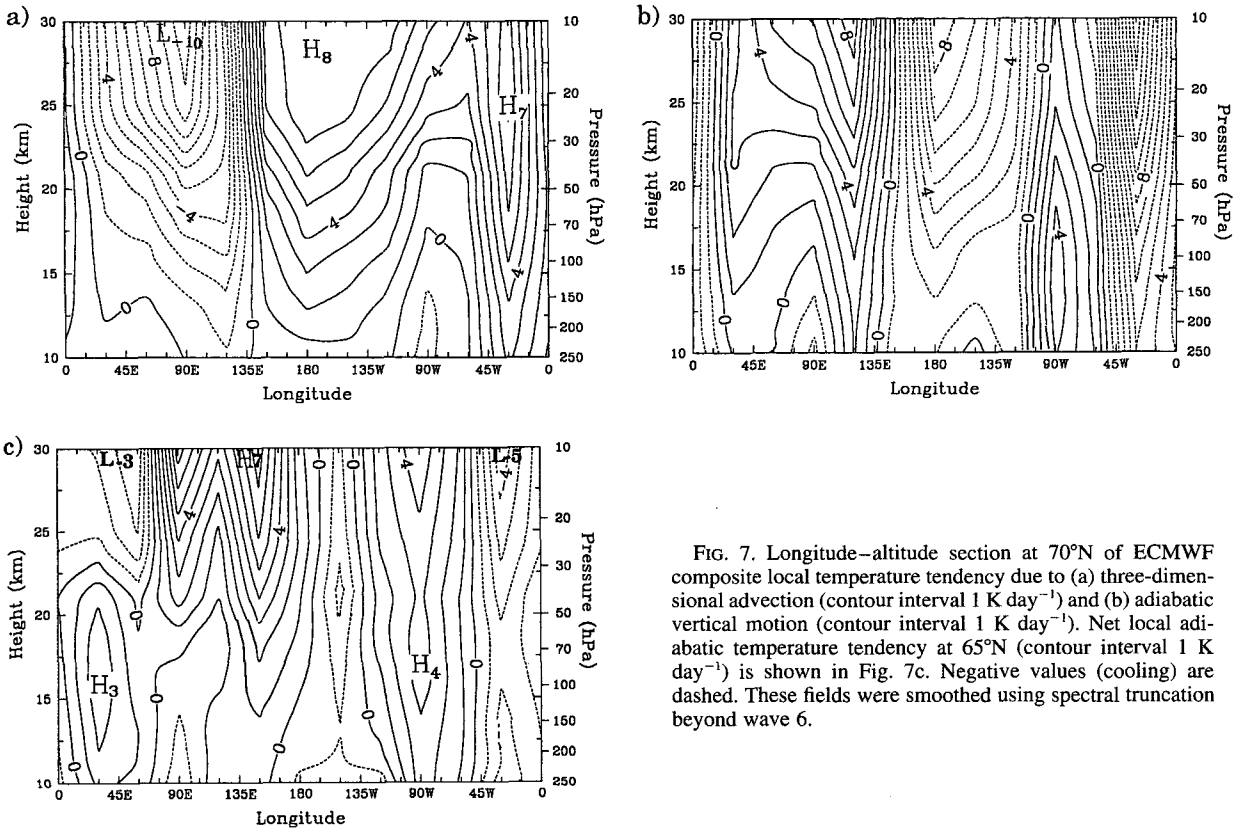

FIG. 7. Longitude–altitude section at 70°N of ECMWF composite local temperature tendency due to (a) three-dimensional advection (contour interval 1 K day^{-1}) and (b) adiabatic vertical motion (contour interval 1 K day^{-1}). Net local adiabatic temperature tendency at 65°N (contour interval 1 K day^{-1}) is shown in Fig. 7c. Negative values (cooling) are dashed. These fields were smoothed using spectral truncation beyond wave 6.

This temperature and wind distribution results in regions of strong thermal advection reaching 15 K day^{-1} in magnitude at 10 hPa (maxima not shown but is apparent qualitatively in Figs. 4b, 6b, and 6c). Figure 7a is a longitude–altitude section at 70°N of three-dimensional temperature advection (cf. section 2). This is slightly south of the warm air advection maximum at 80°N and slightly north of the cold air advection maximum. It can be seen in this plot that warm air advection predominates from ~135° to ~0°E, with cold air advection of similar magnitudes in the eastern hemisphere. Vertical motions exceeding 10 mm s^{-1} are common in this structure, as shown in Fig. 6c. The attendant adiabatic heating and cooling (Fig. 7b) yields warming over Asia and cooling over the Pacific, which tends to compensate the effects of advection. It is difficult to know what extent these dynamically self-consistent vertical motions in the ECMWF analyses are representative of the actual flow fields. These two patterns differ somewhat, and their sum, an estimate of Lagrangian rate of parcel heating, is shown in Fig. 7c. Comparing Figs. 7a and 7b, it may be seen that, near 60°N, subsidence heating overcomes horizontal cold air advection just upstream of the warm anomaly, while ascent cooling overcomes horizontal warm air advection just upstream of the cold anomaly. This is true over a deep vertical layer that extends at least from the middle stratosphere to tropopause levels.

To the extent that this AHC is representative of a steady-state pattern, the pattern of Lagrangian heating provides an estimate of Eulerian net radiative heating rates. For net dynamical heating of 10 K day^{-1} near a thermal anomaly of 10 K, local radiative processes must have surprisingly short timescales, on the order of 1 day. Departures from this steady assumption, of course, are integral to the observed highly transient nature of the AH region. Detailed heat budget studies will be reported elsewhere, but it is useful to note that marked parcel displacements out of radiative equilibrium, and the resulting response, are an essential ingredient in the northern winter general circulation.

The longitude–altitude structure of Lait's PV (Π) for the ECMWF AHC is shown in Fig. 8. It can be seen that the AH is associated with anomalously low PV that amplifies upward, consistent with the hypothesis that part of the AH structure near 10 hPa is due to enhanced advection of low PV air from the Tropics around the polar low.

The AHC eddy geopotential height and temperature structures in NMC data for 1985–1994 are shown at 56°N in Figs. 9a and 9b. Here it can be clearly seen that the AH-polar low pair is vertically continuous from

the surface into the mesosphere, as suggested by Hirota et al. (1973). The tropopause appears to be a node in eddy temperature amplitude, above which some tropospheric features fade and others amplify. Note the upward disappearance of the cold anomaly over the east coast of North America and the pronounced westward tilt with height of the North Atlantic warm anomaly, merging with the warm anomaly over the northeast Pacific. This structure is strikingly similar to the nonlinear numerical simulation results of O'Neill and Pope (1988). Note that the primary trough-ridge pair maximizes near 1.5 hPa at 56°N (even though the criteria is applied at the 10-hPa surface). These figures are certainly consistent with the notion that the AHC structure is causally related to land–sea heating contrasts and topography.

Figures 10a and 10b show the NMC AHC zonal and meridional wind structures at 56°N. The boreal winter extratropics are perhaps best characterized as strongly zonally asymmetric. Zonal eastward flows near 180° are less than 15 m s^{-1} from the midtroposphere into the mesosphere, while they exceed 60 m s^{-1} near 0°E at the stratopause in Fig. 10a. The poleward and equatorward flows are stronger than 20 m s^{-1} in the upper stratosphere in Fig. 10b. Note how the northerly "monsoon" flow over the eastern half of North America extends upward past the stratopause. This AHC meridional wind structure provides useful estimates of preferred longitude bands of meridional mass transport, with a well-defined westward tilt with height.

Differences between ECMWF and NMC eddy composite temperatures and geopotential heights are less than 2 K and 50 m near 56°N. Meridional wind differences are also small, being less than 2 m s^{-1}. Significant differences are seen, however, in zonal mean temperatures and geopotential heights, with values above 50 hPa being 3–7 K warmer and 250–750 m higher in the ECMWF data. The meridional dependence of this

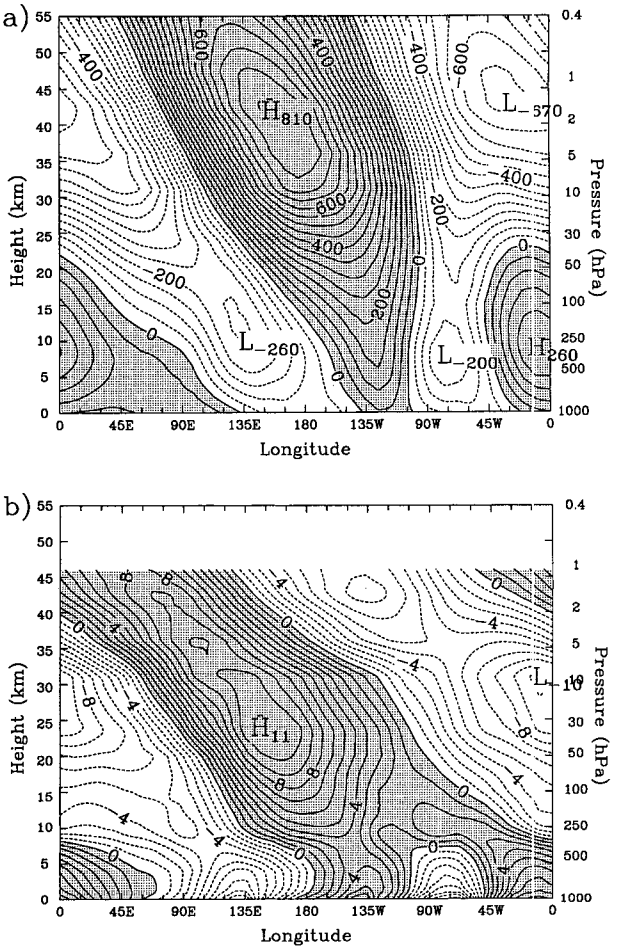

FIG. 9. Longitude–altitude section at 56°N of NMC composite (a) eddy geopotential height (contour interval is 50 m) and (b) eddy temperature (contour interval 1 K). Positive eddy values, which are associated with the Aleutian high (and North Atlantic high in the troposphere) are shaded.

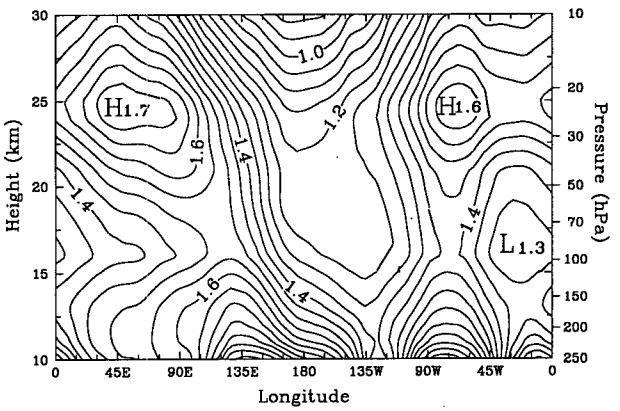

FIG. 8. As in Fig. 6 except of isentropic potential vorticity, where the density dependence is scaled out (see text for further details). Contour interval is 1 × 10^{-6} K m^2 K g^{-1} s^{-1}.

bias is such that, poleward of 35°N and above 50 hPa, ECMWF zonal winds are 5–8 m s^{-1} less westerly. It is the direct application of selected AH days based on ECMWF data which determined the NMC AHC. Clearly, threshold criteria would have to be modified slightly to define the AH from NMC or LIMS data alone.

Since the winter 1978/79 was different than the 1985–1994 winters, differences between LIMS and ECMWF for those two periods do not necessarily indicate biases between the two datasets. Due to the coarser horizontal resolution of the LIMS dataset, the relative vorticity criterion was relaxed to $< -1.5 \times 10^{-5}$ s^{-1}, netting 53 LIMS AHC days, typical of most winters. The Aleutian high intensified from December through January, during which ~50% of the days satisfied the criteria. In February only 6 days were chosen, as multiple SSWs occurred. Longitude–alti-

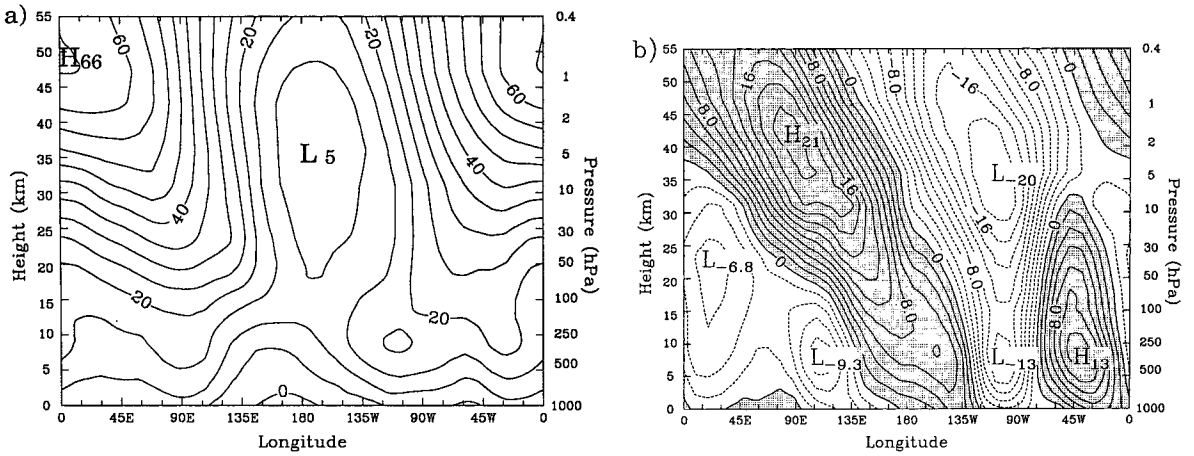

FIG. 10. Longitude–altitude section at 56°N of NMC composite (a) zonal wind (contour interval 5 m s^{-1}), and (b) meridional wind (contour interval 2 m s^{-1}). Positive values denote eastward/northward flow and negative values denote westward/southward flow. In Fig. 10b poleward flow, associated with the displaced polar vortex–Aleutian high in the stratosphere, is shaded.

tude section of LIMS eddy geopotential heights and temperatures at 56°N are shown in Figs. 11a and 11b. There is good agreement with the basic structure seen in Figs. 6a, 6b, 9a, and 9b. Again, maximum eddy heights are seen near 1.5 hPa, rather than 10 hPa. LIMS AHC eddy temperatures maximize near 60 km. Inspection of daily sequences in this limited sample reveals a fair amount of day to day variability in vertical structure, varying from nearly barotropic to a pronounced tilt with height. That winter was quite active in terms of sudden warmings.

An AHC LIMS ozone section is depicted in Fig. 11c. In the stratosphere, high ozone is colocated with the warm AH, despite the tendency to diminish ozone via temperature-dependent reaction rates. This substantiates the concept suggested by the PV distribution, that tropical air with high ozone and low PV is advected eastward around the polar low and incorporated into the AH.

7. Latitude–altitude structure

Although the longitude–altitude sections suggest a planetary wave structure connection of the AH to the extratropical troposphere, it is interesting to examine its latitudinal structure. Figures 12a and 12b show the Northern Hemisphere NMC AHC eddy geopotential heights and temperatures at 175°W and 155°E, transecting their respective maxima. The axis of highest heights trends downward and equatorward to a chronic anticyclone located in the upper troposphere in the western Pacific. A similar structure is seen in eddy temperatures. This tropical upper-tropospheric feature is a well-known aspect of the monsoon structures during boreal winter (Postel 1994). This structure is compatible with upward and equatorward propagation of planetary Rossby wave activity expected from the linear dispersion relation and forcing in the troposphere. Yet it also suggests that a tropical energy source could influence the AH. Some theoretical support for this comes from the work of Simmons (1982), Branstator (1985), and Sardeshmukh and Hoskins (1988).

A complementary view of the AHC structure is obtained by examining NMC temperatures along 155°E and zonal winds along 175°W in a transect over the pole, thence along 30°W and the GM, respectively (Figs. 13a and 13b). Near 60°N through the "warm anomaly" (Fig. 13a) the stratosphere is much more isothermal than at other locations. A poleward tilt with altitude is seen. The associated anticyclonic circulation at 175°W exists in the layer 25–45 km (Fig. 13b). The AH-polar low pair both tilt westward and toward the eastern hemisphere with increasing altitude. In general, winds in the subtropics are quite different for the two longitudes at almost every altitude, supporting the idea that quasi-stationary zonal asymmetries are an essential ingredient to the middle atmosphere general circulation. In particular, the AH helps determine preferred longitude bands of tropical–extratropical exchange that are altitude dependent.

8. Summary and conclusions

A definition of the Aleutian high is proposed involving 5 criteria applicable to ECMWF data, resulting in 711 days for which it clearly existed during the years 1985–1994. An analogous composite is formed for the same 711 days using NMC data. The 5 criteria are applied to the 1978–79 LIMS dataset, resulting in a number of AH days typical for one winter. The NMC and LIMS data are essential in showing the continuous vertical extent of the AH and polar low from the surface into the mesosphere, and the basic structure of the three composites are very similar. Substantial zonal mean bi-

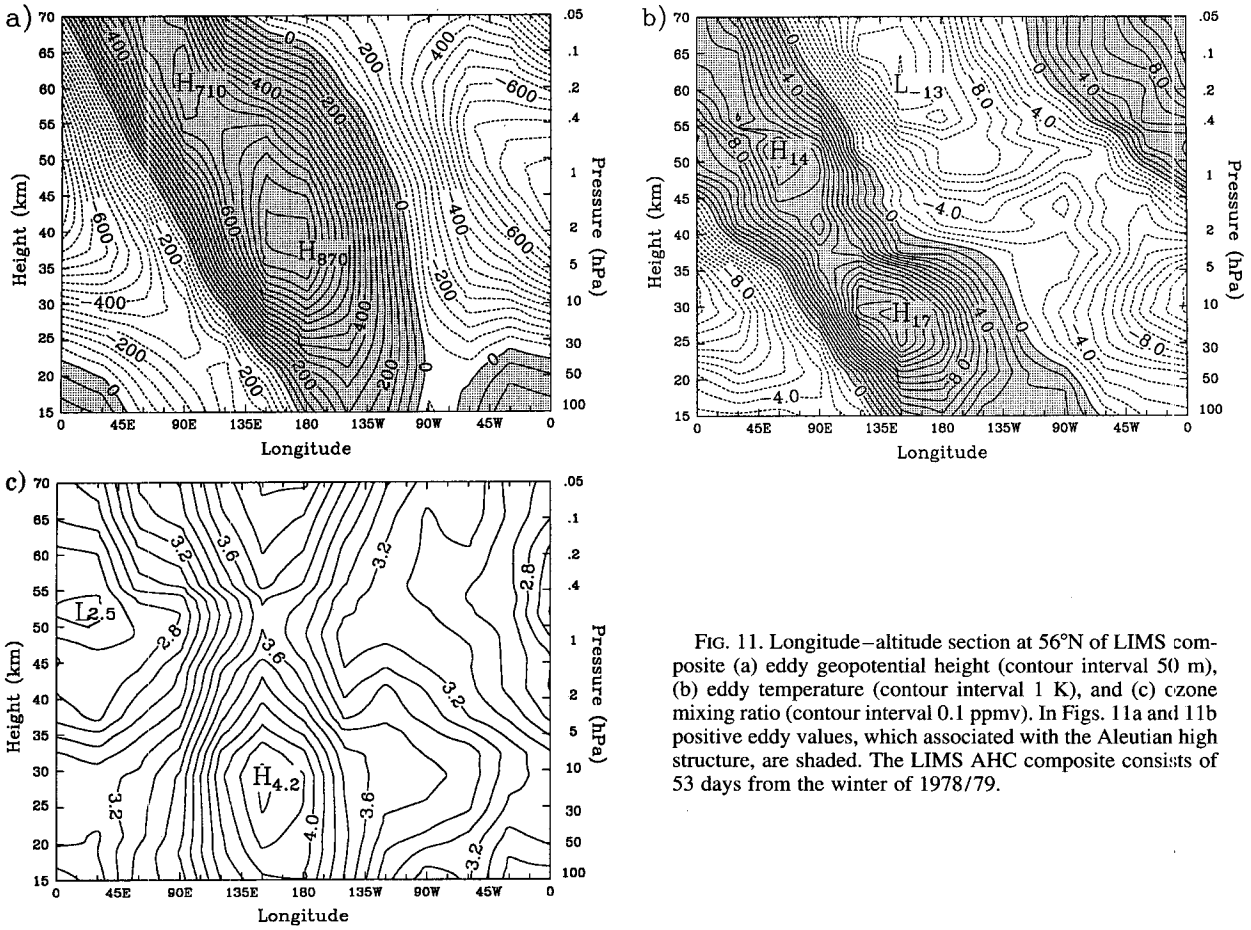

FIG. 11. Longitude–altitude section at 56°N of LIMS composite (a) eddy geopotential height (contour interval 50 m), (b) eddy temperature (contour interval 1 K), and (c) ozone mixing ratio (contour interval 0.1 ppmv). In Figs. 11a and 11b positive eddy values, which associated with the Aleutian high structure, are shaded. The LIMS AHC composite consists of 53 days from the winter of 1978/79.

ases are found in the middle stratosphere, with ECMWF 10-hPa temperatures and geopotential heights being significantly higher than for NMC. In studying the AH in other years for other datasets, therefore, it might be necessary to adjust our proposed criteria accordingly.

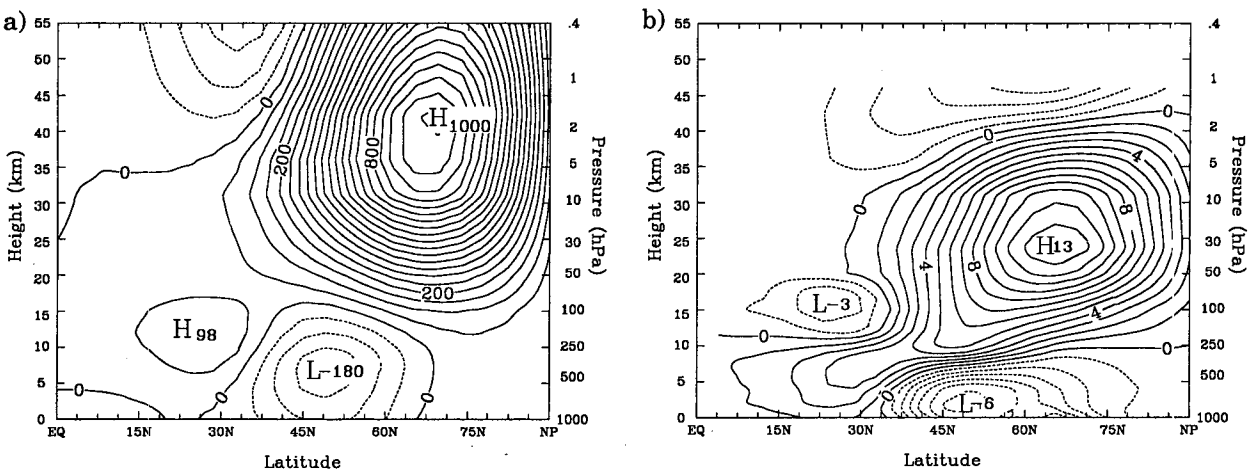

FIG. 12. Latitude–altitude section of NMC composite (a) eddy geopotential height at 175°W (contour interval 50 m) and (b) eddy temperature at 155° E (contour interval 1 K).

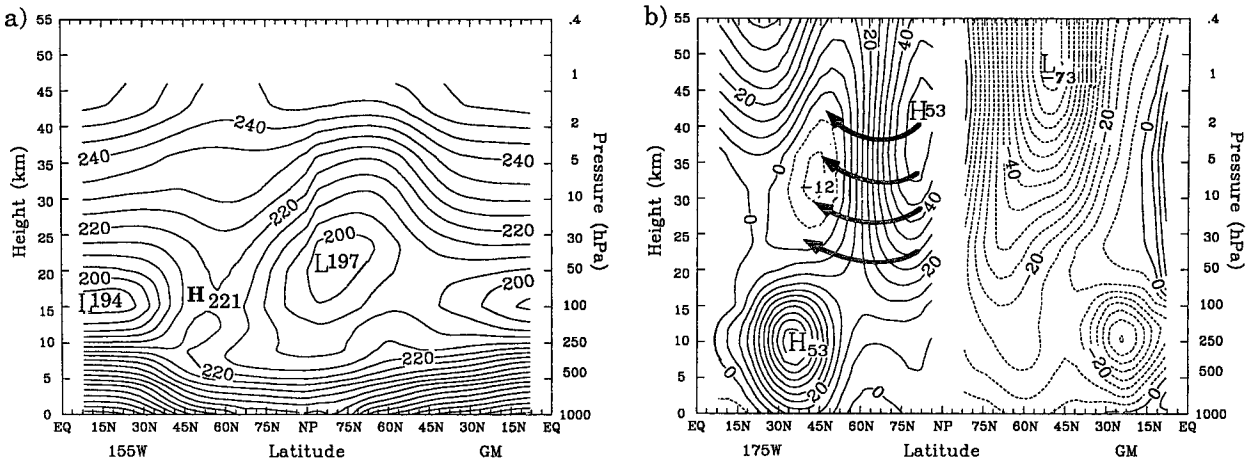

FIG. 13. Latitude–altitude section crossing the North Pole (a) along 155°E (at left) and 30°W (at right) of AHC temperature (contour interval 5 K), and (b) along 175°W (at left) and the GM (at right) of AHC zonal wind (contour interval 5 m s^{-1}). In (b), flow into the diagram (from the viewpoint of the reader) is dashed, and arrows indicate the vertical extent of the anticyclonic circulation that is associated with the Aleutian High.

The AH and polar low tilt westward with altitude and also poleward (again: toward the eastern hemisphere in the stratosphere). The geopotential height difference between the two is ~2.4 km near 10 hPa, is largest near 1.5 hPa, and is much larger than the standard deviation of daily data. This time mean structure shows that the boreal winter is highly zonally asymmetric, with a column of very weak zonal flow within the anticyclone and strong westerlies at other longitudes. Substantial meridional flows define preferred longitude bands of material exchange between low and high latitudes. Subsidence approaching a few cms per second is diagnosed upstream of the warm axis, which underlies the AH in geopotential height.

The AHC structure suggests that the dynamical ingredients that maintain it vary notably with altitude. In the lower stratosphere there appears to be a connection to the tropospheric longwave pattern, but at higher levels there is a nonlinear emergence of the AH–polar vortex pair. Some aspects of this under investigation include analysis of the effects of variability of the tropospheric North Atlantic high and the upward radiation of Rossby wave activity from the east coast of Asia in Plumb fluxes (Plumb 1985). In the middle stratosphere an accretion/merging regime may be a more useful conceptual model, where shallow tongues of low potential vorticity air are advected out of the Tropics around the displaced polar vortex, augmenting the Aleutian high. This, in turn, displaces the polar vortex again, which, with the radiative tendency for strengthening the polar vortex, yields a stably oscillating Aleutian high–polar vortex pair. In the upper stratosphere and lower mesosphere it is likely that gravity wave drag is important in maintaining the Aleutian high. Fritts (1984) gives a thorough review of gravity wave saturation in the middle atmosphere. In the zonal mean it has been established that gravity wave drag caps the polar night jet, yielding poleward and downward flow, with subsidence warming leading to a "separated polar winter stratopause" (Hitchman et al. 1989). This zonal mean feature is intimately related to the AH, as shown by Hirota et al. (1973). Since the 3D zonal wind structure spirals upward around the pole, gravity wave drag should have a similar structure. Intense gravity wave activity has been observed during SSWs as described by Philbrick and Chen (1992). Ongoing work includes an estimation of the relationship among gravity wave drag, winds, temperatures, and heights for the Aleutian High.

Acknowledgments. We are grateful to Chip Trepte for his help in acquiring the datasets. We would also like to thank the reviewers for their helpful comments and suggestions. This work was supported by NASA Grants NAG5-2722, NAS1-19558, and NAGW-2943.

REFERENCES

Baldwin, M. P., X. Cheng, and T. Dunkerton, 1994: Observed correlations between winter-mean tropospheric and stratospheric circulation anomalies. *Geophys. Res. Lett.*, **21,** 1141–1144.

Boville, B. W., 1960: The Aleutian stratospheric anticyclone. *J. Meteor.*, **17,** 329–336.

——, 1963: What are the causes of the Aleutian anticyclone? *Meteor. Abh.*, **36,** 107–120.

Bowman, K. P., and A. J. Krueger, 1985: A global climatology of total ozone from the *Nimbus-7* Total Ozone Mapping Spectrometer. *J. Geophys. Res.*, **90,** 7967–7976.

Branstator, G., 1985: Analysis of general circulation model sea surface temperature anomaly models using a linear model. Part I: Forced solutions. *J. Atmos. Sci.*, **42,** 2225–2241.

Butchart, N., and E. E. Remsberg, 1986: The area of the stratospheric polar vortex as a diagnostic for tracer transport on an isentropic surface. *J. Atmos. Sci.*, **43,** 1319–1339.

Charney, J. P., and P. G. Drazin, 1961: Propagation of planetary-scale disturbances from the lower into the upper atmosphere. *J. Geophys. Res.*, **66,** 83–109.

Chen, P., and W. A. Robinson, 1992: Propagation of planetary waves between the troposphere and stratosphere. *J. Atmos. Sci.*, **49**, 2533–2545.

Da Silva, A. M., and R. S. Lindzen, 1993: On the establishment of stationary waves in the Northern Hemisphere winter. *J. Atmos. Sci.*, **50**, 43–61.

Dickinson, R. E., 1968: Planetary Rossby waves propagating vertically through weak westerly wind wave guides. *J. Atmos. Sci.*, **25**, 984–1002.

Dunkerton, T. J., and D. P. Delisi, 1986: Evolution of potential vorticity in the winter stratosphere of January–February 1979. *Geophys. Res. Lett.*, **91**, 1199–1208.

——, ——, and M. P. Baldwin, 1988: Distribution of major stratospheric warmings in relation to the quasi-biennial oscillation. *Geophys. Res. Lett.*, **15**, 136–139.

Fairlie, T. D. A., M. Fisher, and A. O'Neill, 1990: The development of narrow baroclinic zones and other small-scale structure in the stratosphere during simulated major warmings. *Quart. J. Roy. Meteor. Soc.*, **116**, 287–315.

Farman, J. C., A. O'Neill, and R. Swinbank, 1994: The dynamics of the Arctic polar vortex during the EASOE campaign. *Geophys. Res. Lett.*, **21**, 1195–1198.

Finger, F. G., and S. Teweles, 1963: Synoptic charts based on rocketsonde data. *Meteor. Abh.*, **36**, 379–389.

Fleagle, R. G., 1958: On the dynamics of the general circulation. *Quart. J. Roy. Meteor. Soc.*, **83**, 1–20.

Fritts, D. C., 1984: Gravity wave saturation in the middle atmosphere: A review of theory and observations. *Rev. Geophys.*, **22**, 275–307.

Gille, J. C., and J. M. Russell III, 1984: The Limb Infrared Monitor of the Stratosphere (LIMS) experiment description, performance, and results. *J. Geophys. Res.*, **89**(D4), 5125–5140.

Hamilton, K., 1993a: A general circulation model simulation of El Niño effects in the extratropical Northern Hemisphere stratosphere. *Geophys. Res. Lett.*, **20**, 1803–1806.

——, 1993b: An examination of observed Southern Oscillation effects in the Northern Hemisphere stratosphere. *J. Atmos. Sci.*, **50**, 3468–3473.

Hartmann, S. G., and S. J. Ghan, 1980: A statistical study of the dynamics of blocking. *Mon. Wea. Rev.*, **108**, 1144–1159.

Hirota, I., K. Saotome, T. Suzuki, and S. Ikeda, 1973: Structure and behavior of the Aleutian anticyclone as revealed by meteorological rocket and satellite observations. *J. Meteor. Soc. Japan*, **51**, 353–362.

Hitchman, M. H., and C. B. Leovy, 1986: Evolution of the zonal mean state in the equatorial middle atmosphere during October 1978–May 1979. *J. Atmos. Sci.*, **43**, 3159–3176.

——, J. C. Gille, C. D. Rodgers, and G. Brasseur, 1989: The separated polar winter stratopause: A gravity wave driven climatological feature. *J. Atmos. Sci.*, **46**, 410–422.

——, M. McKay, and C. R. Trepte, 1994: A climatology of stratospheric aerosol. *J. Geophys. Res.*, **99**, 20 689–20 700.

Hofmann, D. J., and J. M. Rosen, 1984: Balloon-borne particle counter observations of the El Chichon aerosol layers in the 0.01–1.8 μm radius range. *Geofis. Int.*, **23**, 155–185.

Holton, J. R., and H.-C. Tan, 1980: The influence of the equatorial quasi-biennial oscillation on the global circulation at 50 mb. *J. Atmos. Sci.*, **37**, 2200–2208.

——, and ——, 1982: The quasi-biennial oscillation in the Northern Hemisphere lower stratosphere. *J. Meteor. Soc. Japan*, **60**, 140–147.

Hoskins, B. J., and D. Karoly, 1981: The steady linear response of a spherical atmosphere to thermal and orographic forcing. *J. Atmos. Sci.*, **38**, 1179–1196.

Juckes, M. N., and A. O'Neill, 1988: Early winter in the northern stratosphere. *Quart. J. Roy. Meteor. Soc.*, **114**, 1111–1125.

Julian, P. R., and K. Labitzke, 1965: Study of atmospheric energetics during the Jan.–Feb. 1963 stratospheric warming. *J. Atmos. Sci.*, **22**, 597–610.

Julian, R. R., 1963: Some correlations of tropospheric and stratospheric pressure and temperature in mid- and high-latitudes. *Meteor. Abh.*, **36**, 63–75.

Kaas, E., and G. Branstator, 1993: The relationship between a zonal index and blocking activity. *J. Atmos. Sci.*, **50**, 3061–3077.

Karoly, D. J., and B. J. Hoskins, 1982: Three-dimensional propagation of planetary waves. *J. Meteor. Soc. Japan*, **60**, 109–122.

Kasahara, A., T. Sasamori, and W. Washington, 1973: Simulation experiments with a 12-layer stratospheric global circulation model. Part I: Dynamical effect of the earth's orography and thermal influence of continentality. *J. Atmos. Sci.*, **30**, 1229–1251.

Kiehl, J. T., and S. Solomon, 1986: On the radiative balance of the stratosphere. *J. Atmos. Sci.*, **43**, 1525–1534.

Kitaoka, T., 1963: Some considerations of the stratospheric circulation, related to the cause of the Aleutian high. *Meteor. Abh.*, **36**, 121–152.

Labitzke, K., 1972: Climatology of the stratosphere in the Northern Hemisphere. Part 1: *Meteor. Abh.*, **100**, 29 pp. + diagrams and tables.

——, 1977: Interannual variability of the winter stratosphere in the Northern Hemisphere. *Mon. Wea. Rev.*, **105**, 762–770.

——, 1980: Climatology of the stratosphere and mesosphere. *Philos. Trans. Roy. Soc. London*, **296**, 7–18.

——, 1981: Stratospheric–mesospheric midwinter disturbances: A summary of observed characteristics. *J. Geophys. Res.*, **86**, 9665–9678.

——, 1982: On the interannual variability of the middle stratosphere during the northern winters. *J. Meteor. Soc. Japan*, **60**, 124–139.

Lait, L. R., 1994: An alternative form for potential vorticity. *J. Atmos. Sci.*, **51**, 1754–1759.

Lin, B.-D., 1982: The behavior of winter stationary planetary waves forced by topography and diabatic heating. *J. Atmos. Sci.*, **39**, 1206–1226.

Manney, G. L., A. O'Neill, and R. Swinbank, 1994a: On the motion of air through the stratospheric polar vortex. *J. Atmos. Sci.*, **51**, 2973–2994.

——, R. W. Zurek, A. O'Neill, R. Swinbank, J. B. Kumer, J. L. Mergenthaler, and A. E. Roche, 1994b: Stratospheric warmings during February and March 1993. *Geophys. Res. Lett.*, **21**, 813–816.

McIntyre, M. E., 1982: How well do we understand the dynamics of stratospheric warmings? *J. Meteor. Soc. Japan*, **60**, 37–65.

——, and T. N. Palmer, 1983: Breaking planetary waves in the stratosphere. *Nature*, **305**, 593–599.

——, and ——, 1984: The "surf zone" in the stratosphere. *J. Atmos. Terr. Phys.*, **46**, 825–849.

Nigam, S., and R. S. Lindzen, 1989: The sensitivity of stationary planetary waves to variations in the basic state zonal flow. *J. Atmos. Sci.*, **46**, 1746–1768.

O'Neill, A., and V. D. Pope, 1988: Simulations of linear and nonlinear disturbances in the stratosphere. *Quart. J. Roy. Meteor. Soc.*, **114**, 1063–1110.

——, and ——, 1993: The coupling between radiation and dynamics in the stratosphere. *Adv. Space Res.*, **13**, 351–358.

——, W. L. Grose, V. D. Pope, H. Maclean, and R. Swinbank, 1994: Evolution of the stratosphere during northern winter 1991/92 as diagnosed from U.K. meteorological office analyses. *J. Atmos. Sci.*, **51**, 2800–2817.

Perlwitz, J., and H. F. Graf, 1995: The statistical connection between tropospheric and stratospheric circulation of the Northern Hemisphere in winter. *J. Climate*, **8**, 2281–2295.

Philbrick, C. R., and B. Chen, 1992: Transmission of gravity waves and planetary waves in the middle atmosphere based on lidar and rocket measurements. *Adv. Space Res.*, **12**, 303–306.

Pierce, R. B., W. T. Blackshear, T. D. Fairlie, W. L. Grose, and R. E. Turner, 1993: The interaction of radiative and dynamical processes during a simulated sudden stratospheric warming. *J. Atmos. Sci.*, **50**, 3829–3851.

Plumb, R. A., 1985: On the three-dimensional propagation of stationary waves. *J. Atmos. Sci.*, **42,** 217–229.

——, D. W. Waugh, R. J. Atkinson, P. A. Newman, L. R. Lait, M. R. Schoeberl, E. V. Browell, A. J. Simmons, and M. Loewenstein, 1994: Intrusions into the lower stratospheric Arctic vortex during the winter of 1991–1992. *J. Geophys. Res.*, **99,** 1089–1105.

Postel, G. A., 1994: Zonally asymmetric large-scale dynamics in the upper troposphere and lower stratosphere. M.S. thesis, University of Wisconsin–Madison, 77 pp.

Quiroz, R. S., 1986: The association of stratospheric warmings with tropospheric blocking. *J. Geophys. Res.*, **91,** 5277–5285.

Randel, W. J., J. C. Gille, A. E. Roche, J. B. Kumer, J. L. Mergenthaler, J. W. Waters, E. F. Fishbein, and W. A. Lahoz, 1993: Stratospheric transport from the Tropics to middle latitudes by planetary-wave mixing. *Nature,* **365,** 533–535.

Reed, R. J., A. Hollingsworth, W. A. Heckley, and F. Delsol, 1986: An evaluation of the performance of the ECMWF operational forecasting system in analysing and forecasting tropical easterly wave disturbances. Part 1: Synoptic investigation. ECMWF Tech. Rep. 58, 74 pp.

Rosier, S. M., B. N. Lawrence, D. G. Andrews, and F. W. Taylor, 1994: Dynamical evolution of the northern stratosphere in early winter 1991–92, as observed by the improved stratospheric and mesospheric sounder. *J. Atmos. Sci.,* **51,** 2783–2799.

Sardeshmukh, P. D., and B. J. Hoskins, 1988: The generation of global rotational flow by steady idealized tropical divergence. *J. Atmos. Sci.,* **45,** 1228–1251.

Schoeberl, M. R., L. R. Lait, P. A. Newman, and J. E. Rosenfield, 1992: The structure of the polar vortex. *J. Geophys. Res.,* **97,** 7859–7882.

Shiotani, M., 1986: Planetary wave activity in the troposphere and stratosphere during the Northern Hemisphere winter. *J. Atmos. Sci.,* **43,** 3200–3209.

Simmons, A. J., 1982: The forcing of stationary wave motion by tropical diabatic heating. *Quart. J. Roy. Meteor. Soc.,* **108,** 503–534.

Stroud, W. G., W. Nordberg, and W. R. Bandeen, 1959: Rocket-grenade observation of atmospheric heating in the Arctic. *J. Geophys. Res.,* **64,** 1342–1343.

Teweles, S., 1958: Anomalous warming of the stratosphere over North America in early 1957. *Mon. Wea. Rev.,* **86,** 377–396.

Trenberth, K. E., 1992: Global analyses from ECMWF and atlas of 1000 to 10 mb circulation statistics. NCAR Tech. Note NCAR/TN-373+STR, 191 pp.

——, and J. G. Olson, 1988: Intercomparison of NMC and ECMWF global analyses. NCAR Tech. Note NCAR/TN-300+STR, 94 pp.

Trepte, C. R., and M. H. Hitchman, 1992: Tropical stratospheric circulation deduced from satellite aerosol data. *Nature,* **355,** 626–628.

van Loon, H., and K. Labitzke, 1987: The Southern Oscillation. Part V: The anomalies in the lower stratosphere of the Northern Hemisphere in winter and a comparison with the quasi-biennial oscillation. *Mon. Wea. Rev.,* **115,** 357–369.

——, and D. J. Shea, 1992: Atlas of point correlations at 30 mb and between 500 and 30 mb. *Bull. Amer. Meteor. Soc.,* **73,** 2010–2012.

——, R. A. Madden, and R. L. Jenne, 1975: Oscillations in the winter stratosphere. Part 1: Description. *Mon. Wea. Rev.,* **103,** 154–162.

Wada, H., 1968: Some interrelationships of large-scale circulation patterns in the troposphere and stratosphere. *J. Meteor. Res.,* **20,** 109–120.

Wallace, J. M., and D. S. Gutzler, 1981: Teleconnections in the geopotential height field during the Northern Hemisphere winter. *Mon. Wea. Rev.,* **109,** 784–812.

——, and F.-C. Chang, 1982: Interannual variability of the wintertime polar vortex in the Northern Hemisphere middle stratosphere. *J. Meteor. Soc. Japan,* **60,** 149–155.

Waugh, D. W., 1993: Subtropical stratospheric mixing linked to disturbances in the polar vortices. *Nature,* **365,** 535–537.

——, R. A. Plumb, R. J. Atkinson, M. R. Schoeberl, L. R. Lait, P. A. Newman, M. Loewenstein, D. W. Toohey, L. M. Avallone, C. R. Webster, and R. D. May, 1994: Transport out of the lower stratospheric Arctic vortex by Rossby wave breaking. *J. Geophys. Res.,* **99,** 1071–1088.

Wilson, C. V., and W. L. Godson, 1963: The structure of the arctic winter stratosphere over a 10-yr. period. *Quart. J. Roy. Meteor. Soc.,* **89,** 205–224.